

# Crack patterns in drying protein solution drops

C. C. Annarelli, J. Fomazero, J. Bert and J. Colombani

Département de Physique des Matériaux – Bâtiment Brillouin  
 Université Claude Bernard Lyon 1  
 6, rue Ampère, F-69622 Lyon-Villeurbanne cedex, France

the date of receipt and acceptance should be inserted later

**Abstract.** A deposited drop of bovine serum albumin in salt solution experiences both gelation and fracture during evaporation. The cracks appearing at the edge of the gelling drop are regularly spaced, due to the competition between the evaporation-induced and relaxation-induced stress evolution. Subsequently, the mean crack spacing evolves in an unexpected way, being inversely proportional instead of proportional to the deposit thickness. This evolution has been ascribed to the change with time of the average shrinkage stress, the crack patterning being purely elastic instead of evaporation-controlled.

PACS. 62.20.Mk, 47.54.+r, 82.70.Gg

## 1 Introduction

The study of crack dynamics in drying materials meets the basic interest in nonequilibrium pattern formation and the industrial need of controlling drying processes (paint technology, ...). But whereas the understanding of crack behaviours is growing, partly due from the interplay between mechanics and statistical physics approaches [1], the investigation of the cracking of drying complex fluids is just setting in.

As part of a general study of biocompatibility between prosthetic materials and real biological liquids, we focussed on the evaporation of a protein solution drop and on the evolution of the solid deposit. Although the gelation process of our biological liquid and the initial stage of the crack pattern formation show similarities with like phenomena in mineral colloids [2,3], the characteristics of our experiments yield further insight in the following steps of the cracking.

Our working liquid is a phosphate buffered saline solution (pH = 7.4, ionic strength  $I = 0.2 \text{ M}$ ) of bovine serum albumin (BSA) at various concentrations, which may be classified as a colloidal solution with the BSA molecules amounting to ellipsoidal particles of dimensions  $4 \times 4 \times 14 \text{ nm}^3$  [4]. The volume fraction of protein is always a few percents in our concentration range. In the course of the experiment, a  $15 \text{ mm}^3$  sessile drop is deposited onto a glass slide. Great care is taken for the cleaning of the substrate, residual deposits being liable to disturb the wetting and cracking behaviour. Keeping in the surface tension-driven regime, tensile drops have been experienced to exhibit the same behaviour. Immediately, proteins are adsorbed on

the substrate, leading to a strong anchoring of the triple line [5].

The first step of dessication is then characterized by a fixed base radius of the drop, a constant evaporation rate all over its free surface and a spherical cap shape induced by surface tension (Bond number smaller than one). These three features have been shown to remain compatible thanks to outward flows inside the drop [6]. Subsequently an apparently solid ring-like "foot" progressively forms close to the edge of the drop, and the three phase line migrates inwards, provoking the extension of the solid until complete dessication.

Due to the competition between the adhesion of the deposit on the substrate and its evaporation-induced orthoradial shrinkage, the foot rapidly experiences regularly-spaced radial cracks (see Figure 1). The periodicity of the fractures in such evaporating colloidal solutions has turned out to originate in the interplay between the stress relaxation induced by the crack and the stress enhancement yielded by the water drainage from the inner liquid to the crack surface [7].

But unlike the case of mineral colloids, the subsequent evolution of our crack pattern is characterized by the stop of a growing number of fractures, always preceded by a right angle turn. In the same time, purely orthoradial cracks appear (see Figure 2). Finally all radial fractures cease to propagate simultaneously and, depending on the protein concentration, two scenarios may occur in the central zone: small-scaled disordered fracturation or dendritic crystallisation (see Figure 3 and [8]). Respective behaviours as a function of the BSA concentration are gathered in Table 1.

## 2 Dynamics

Before studying the fracturation, we concentrate on the evaporation dynamics. To evaluate our dessication time  $\tau_D = \frac{R_0}{v_E}$  with  $v_E = \frac{1}{S} \frac{dV}{dt}$  (water flux per unit surface ( $R_0$  initial base radius,  $S$  surface and  $V$  volume of the drop)), we have performed measurements of the evolution of the drying drop height  $h$  with time  $t$  (see Figure 4). Considering a constant base radius and a spherical cap shape and choosing for  $S$  the overall free surface of the drop, including the foot where evaporation still takes place [2], the dessication time can simply be written  $\tau_D = \frac{2R_0}{(\frac{dh}{dt})_{t=0}} = 1.3 \cdot 10^4$  s.

Furthermore, weighing measurements shown in Figure 5 have brought an additional evaluation of the dessication time with the above-mentioned assumptions:  $\tau_D = \frac{R_0 S_0}{(\frac{dm}{dt})_{t=0}}$  with  $S_0$  the initial air-drop surface,  $m$  the mass of the drop and the density of the solution, determined by picnometry. The obtained numerical value  $\tau_D = 1.5 \cdot 10^4$  s fits with the previous determination. As can be stated in Figure 5, evaporation dynamics compares tightly in pure water and protein solution. Indeed, the volume fraction of the protein keeping small,  $\tau_D$  is quite independent of the BSA concentration.

Then we have focussed on the properties of the solid deposit. Such protein solutions are known to gel during dessication, helped by the increasing ionic strength [9]. To check the physical nature of the obtained biopolymer gel, we placed the slide in water and observed complete redilution of the deposit. Measurements of adsorption spectra and surface tension of the sol before and after the gelation and redilution process give identical results, proof of the non-chemical nature of the bonds in the solid.

To evidence the sol-gel transition kinetics, we have carried out electrical conductivity measurements of the evaporating drop by placing electrodes on the slide, at two edge points of the drop. As can be seen on Figure 6, the progressive hindering of ionic conduction through the liquid by the connection of the protein molecules gives rise to a decrease in the current. We have taken as gelation time  $\tau_G$  the elapsed time at the achievement of the low-conductivity plateau.  $\tau_G$  is found to decrease smoothly when concentration rises (see Table 1).

Finally the cracking characteristic time at which the first fracture is detected has been measured and found quite independent of concentration:  $\tau_C = 8 \cdot 10^2$  s.

## 3 Initial cracking

We now point out the fracturing behaviour of the gel. The fact that the central part of the drop remains liquid and the three phase line anchored while the foot starts shrinking results in orthoradial stress, then in radial cracks. In a quantitative theory of the 1D fracturing behaviour of a mineral colloidal suspension confined in a Hele-Shaw cell, Lin et al. [1] have found that the crack spacing should be roughly proportional to the cell thickness [7]. We have

implemented this model for our open geometry, considering that the same stress field exists in our drop foot as in one longitudinal half of their slab, leading to an equivalent cell thickness of twice the foot height. The theoretical and experimental initial crack spacings  $\lambda_0$  are reported in Table 1. Considering the degree of approximation of the model and the difficulty for the physical parameters evaluation, agreement is found satisfactory.

The foot heights listed in Table 1 have been measured with a holographic interferometry device, thanks to an original geometrical analysis [10]. With this technique, a reference hologram of the studied surface is first recorded with the use of two beams (reference and object), the incident angle of the object beam being  $\theta$ . This hologram contains information on the amplitude and phase of the reflected object beam, enabling a 3D reconstruction of the surface. Then a mirror is tilted, changing the incident angle of the object beam to  $\theta + \alpha$  and a new hologram is recorded. The interference of the two holograms results in a fringe pattern, an example of which is shown in Figure 7. We have shown in [10] that at surfaces lead to fringes parallel to the tilt axis, whereas any defect of height  $m$  in the surface creates a fringe shift  $p$  with  $p = m \tan(\theta + \alpha)$ . The deposit topography has therefore been derived from the measurement of the fringes deviation on the interference pattern caused by a tilt  $\alpha = 0.5^\circ$  from the incident angle  $\theta = 80^\circ$ . Validation of the results have been provided by complementary profilometry measurements. This method has moreover permitted to check that the flatness of the slide was better than 2  $\mu$ m over the distances investigated here.

## 4 Cracking evolution

After the initial breaking, number of cracks merge during propagation and the mean crack spacing  $\lambda$  may increase. In the vicinity of a crack, the stress is purely parallel to its edges, so when a radial fracture tends to stop, it experiences a turn to join an adjacent one with a right angle. The evolution of the mean crack spacing  $\lambda$  (taken as the ratio of a perimeter to the number of fractures crossing it) when going from the center to the edge of the dried drop is shown in Figures 8 and 9 with same scales for 40 and 60 g.l<sup>-1</sup> BSA concentrations.

As has been qualitatively [11] and quantitatively (see above) demonstrated in different configurations, the crack spacing should be roughly proportional to the layer thickness. We have therefore used our holographic interferometry measurements to get informations about the thickness of the deposit along the radius of the dried drop. Results are represented in Figures 8 for the 40 g.l<sup>-1</sup> case and 9 for the 60 g.l<sup>-1</sup> case and give a clear view of the fact that the link between crack vanishing and layer thickness is different from what could be expected.

In fact, if we evaluate the characteristic time of diffusion of water in the gel between two cracks during the initial stage, the order of magnitude is found greater than 10 minutes, i.e., comparable to the whole fracturation time ( $\sim 15$  min.). So after the initial cracking, evaporation

ceases to constitute a leading feature of the phenomenon. Therefore we must now look back at the involved kinetics to assess the governing mechanism.

## 5 Crack pattern

For an identical time hierarchy ( $t_c < t_g < t_d$ ), Pauchard et al. observed disordered crack patterns during the evaporation of an aqueous silica sol deposited drop, caused by a buckling instability [3]. This one consists of a distortion of the drop shape caused by the gelation of the surface when the inner sol is still liquid. We do not face this morphological behaviour, the central zone solidifying progressively through the propagation of the gel front.

Before ascribing this discrepancy to the respective natures of the mineral and biopolymer gels, the influence of the geometrical parameters has to be investigated. Showing an axial symmetry, only two dimensions have to be probed. First the drop volume has been varied from 2 to 25 mm<sup>3</sup> with solutions of concentrations 20 to 60 g.l<sup>-1</sup>. Then, for identical concentrations, the contact angle has been changed by testing several substrates of biomedical interest, the wettability characteristics of which had already been studied [5]: nitrogen implanted (59°) and virgin (62°) titanium based alloy TA 6V, GUR 415 (65°) and Chirulen (67°) ultra high molecular weight polyethylenes, sintered alumina (66°) and zircona (67°), stainless steel 316L (68°), and a chromium-cobalt alloy (71°). Additionally, silane-coated glass (> 90°) has been tested. Whereas the fractures penetration depth variation with concentration and contact angle show interesting features [which will be studied elsewhere], in all cases the drop morphology and cracking evolution are similar to the case of the 15 mm<sup>3</sup> drop deposited on glass. One only difference can be noticed for volumes smaller or equal to 5 mm<sup>3</sup> and silane-coated glass where all initial radial fractures stop propagating at the same time instead of hierarchically due to the small base radius of the drop.

So the universal radial nature of the crack pattern (instead of a disordered nature for a mineral gel) seems to be independent of geometrical considerations and can reasonably be attributed to the physical nature of the biopolymer gel, the latter exhibiting smoother mechanical properties than chemical gels. Its low tensile strength in the gelling central zone should thereby result in an overall stress in the gel front keeping an orthoradial direction.

## 6 Mean crack spacing evolution

The dessication kinetics being non-critical after the initial cracking, information is now transmitted elastically between cracks, through the flux of displacement field, as pointed out in impact fracture experiments [12], which is a much faster mode. Thus we face a pattern selection system comparable to the one encountered in thermal crack growth experiments [13]: The release of elastic energy during the propagation controls the crack spacing.

Indeed for the propagation of a crack to be possible, the elastic energy  $E_e$  liberated by the breaking must at least equal the surface energy  $E_s$  required by the two formed lips (Griffith's criterion). We are considering here as a first approximation purely brittle breaking, dissipative effects (plasticity, friction) being neglected. During the progression of a fracture,  $E_e$  is proportional to the relaxed volume  $e_{rel}$  and  $E_s$  to the created surface area  $e_{surf}$ . So the fulfilment of the  $E_e = E_s$  condition does not imply, in the case of a change of  $e$ , a modification of the crack spacing. Therefore the evolution of  $e$  when approaching the center of the drop, if any, should be related to a change in the only other varying factor along the fracture path: the stress field.

For example, in the 40 g.l<sup>-1</sup> case,  $e$  evolves roughly as  $r^{-\frac{1}{2}}$  ( $r$  distance from the center of the drop), so linear elasticity yields a change of the stress proportional to  $r^{-\frac{1}{2}}$  so to  $r^{\frac{1}{2}}$ . This slow decrease of  $e$  when going from the edge to the center of the drop has to be related to the decrease of the average stress with time: Cracks meet during their propagation a gel more and more relaxed by the continuous fracturation [14]. In the 60 g.l<sup>-1</sup> case,  $e$  exhibits no actual evolution, which should stem from a constant stress during the cracking process. This constancy of the stress is likely to be a consequence of the large and quite uniform layer thickness, which hinders relief mechanisms.

So the dynamics of the mean crack spacing has revealed itself to be actually related to the deposit thickness, but not in the expected way: It is rather inversely proportional instead of proportional. Indeed, dessication playing no more role, only cracking influences the cracking geometry through stress relief, which is made easier by decreasing layer thicknesses.

## 7 Conclusion

We have investigated the evaporating, gelling and cracking behaviour of a deposited drop of protein solution. The initial stage is characterized by the appearance of regularly-spaced cracks at the edge of the gelling drop. This ordered patterning was known to originate in the interplay between the water diffusion towards the crack surface and the elastic relaxation due to the fracture. The general radial patterning was found to be a corollary of the soft nature of the BSA gel. Then a transition from this evaporation-controlled behaviour to a purely elastic one occurs, where the change of the crack spacing has turned out to be a consequence of the shrinkage stress evolution with time.

This first study of the fracturing behaviour of a drying biological liquid has shown similarities with other complex fluids. But discrepancies have also been emphasized and an investigation of the specific mechanical properties of the biopolymer gel is still needed to confirm the assumptions made on the dynamics of the fracturation. The influence of the substrate on the cracking, especially on fracture penetration depths, constitutes also a promising way of investigation.

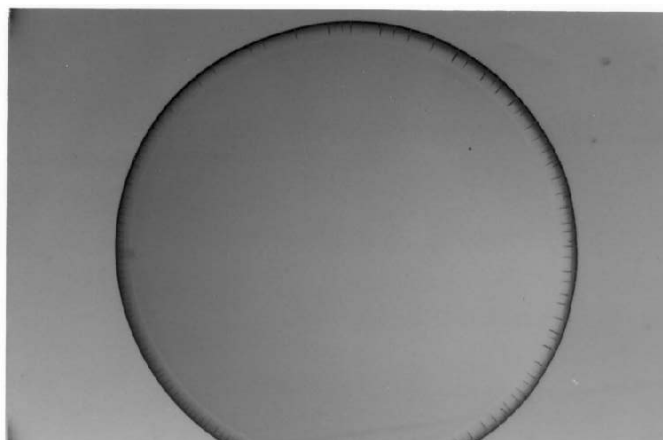


Fig. 1. Beginning of the foot fracturation of a drying 40 g.l<sup>-1</sup> solution drop 840 s after deposit.

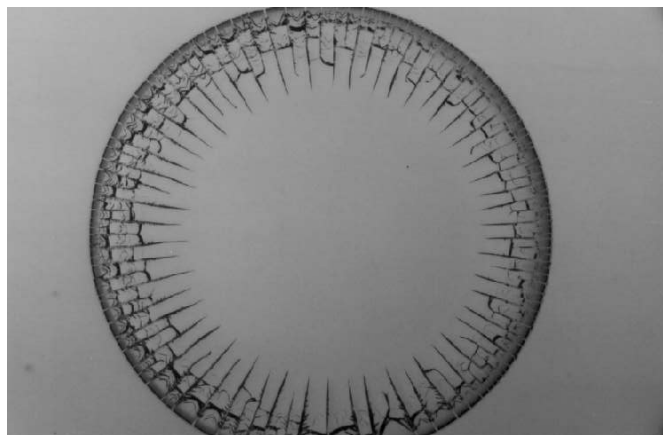


Fig. 2. Following of the fracturation of the drying drop of Figure 1, 500 s later.

We acknowledge fruitful discussions with Laurence Reyes and Christian Oignon and experimental help from Richard Cohen, Jean-Alexandre Roger and Stella Ramos-Canuto.

## References

1. J. Charmet, S. Roux, and E. Guyon, NATO ASI Series B: Physics - Disorder and fracture (Plenum press, New York, 1990), Vol. 235.
2. F. Parisse and C. Allain, *Langmuir* 13, 3598 (1997).
3. L. Pauchard, F. Parisse, and C. Allain, *Phys. Rev. E* 59, 3737 (1999).
4. T. Peters, *Adv. Protein Chem.* 37, 161 (1985).
5. C. Annarelli et al., *J. Colloid Interface Sci.* 213, 386 (1999).
6. R. Deegan et al., *Nature* 389, 827 (1997).
7. C. Allain and L. Limat, *Phys. Rev. Lett.* 74, 2981 (1995).
8. C. Annarelli et al., *Cryst. Eng.* 2, 79 (1999).
9. S. Magdassi, *Surface activity of proteins: chemical and physicochemical modifications* (Marcel Dekker, Jerusalem, 1996).
10. C. Annarelli, Ph.D. thesis, Université Claude Bernard Lyon 1, 1998.
11. A. Gershanik and E. Kaplan, *Europhys. Lett.* 25, 415 (1994).
12. H. Inaoka and H. Takayasu, *Physica A* 229, 5 (1996).
13. O. Ronsin and B. Perrin, *Europhys. Lett.* 38, 435 (1997).
14. A. Skjeltrop and P. Meakin, *Nature* 335, 424 (1988).

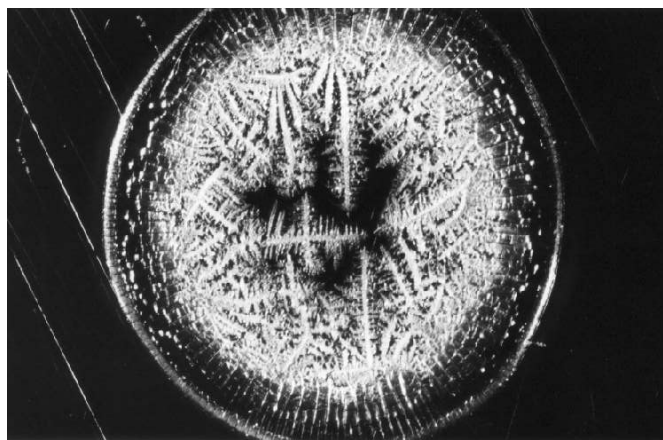


Fig. 3. Dendritic crystallisation of the central zone of a dried 10 g.l<sup>-1</sup> solution drop.

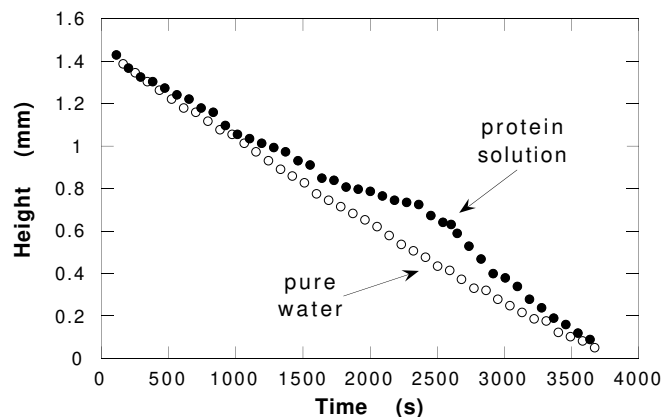


Fig. 4. Time evolution of a drying 40 g.l<sup>-1</sup> solution drop height. As a matter of comparison the values for a pure water drop are also displayed.

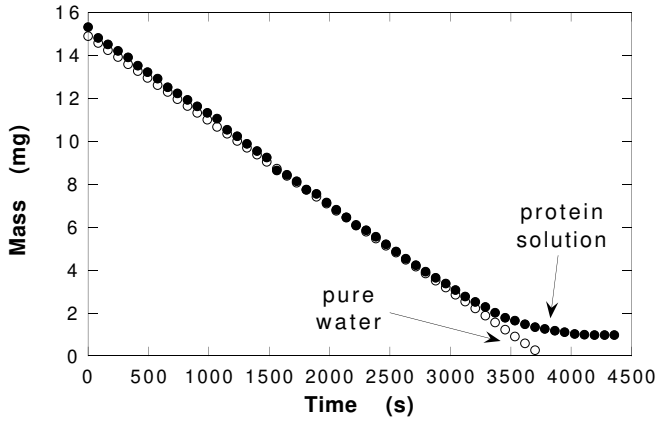


Fig. 5. Time evolution of a drying  $40 \text{ g.l}^{-1}$  solution drop mass. Values for pure water are also displayed.

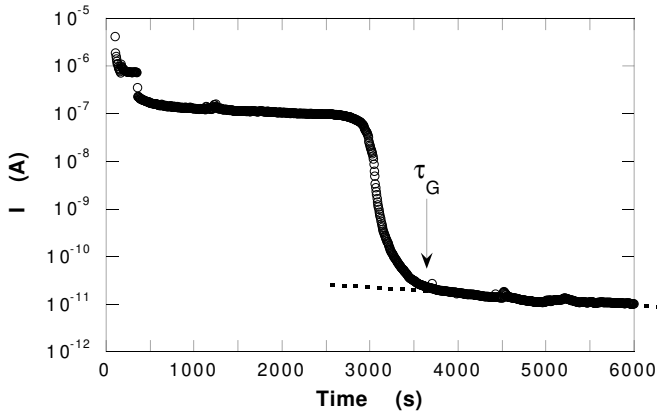


Fig. 6. Time evolution of the electric current between two edge points of the drying  $40 \text{ g.l}^{-1}$  solution drop.

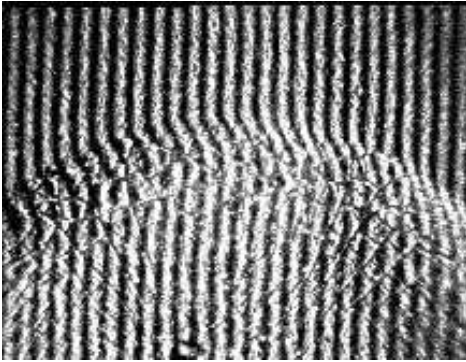


Fig. 7. Holo interferogram of a dried  $40 \text{ g.l}^{-1}$  drop deposit.

$c$ ( $\text{g.l}^{-1}$ )	foot height ( $\mu\text{m}$ )	$\tau_G$ ( $10^3 \text{ s}$ )	$\tau_0^{\text{exp}}$ ( $\mu\text{m}$ )	$\tau_0^{\text{theo}}$ ( $\mu\text{m}$ )	nalbehaviour
20	28	3.8	100	124	crystallisation
30	31	3.7	120	135	crystallisation
40	36	3.6	160	154	fracturation
60	81	3.4	250	309	fracturation

Table 1. Foot height, gelation characteristic time, experimental value of the initial crack spacing, theoretical value of the initial crack spacing, nalbehaviour of the deposit center as a function of BSA concentration.

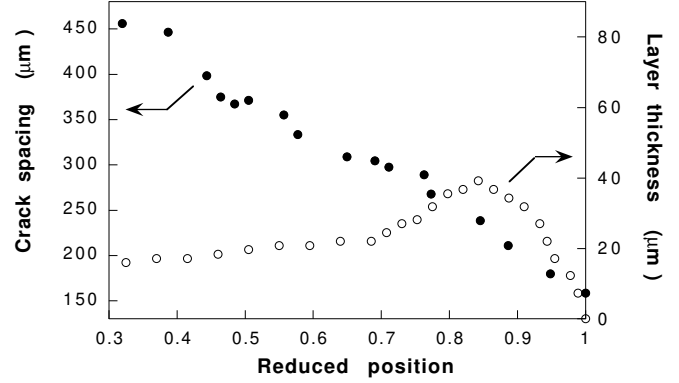


Fig. 8. Layer thickness  $e$  and crack spacing as a function of the reduced distance  $r=R_0$  from the center of a dried  $40 \text{ g.l}^{-1}$  drop.

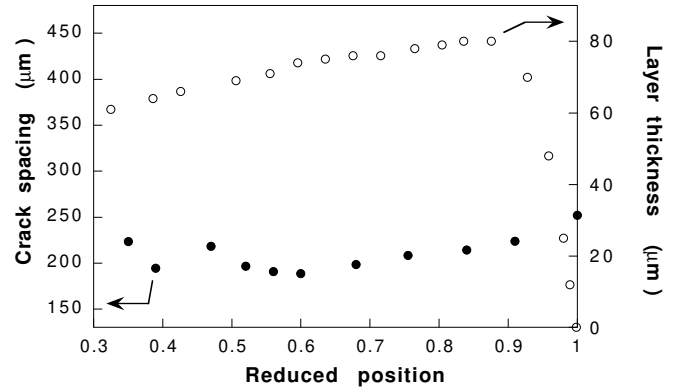


Fig. 9. Identical to Figure 8 (same scales) for a dried  $60 \text{ g.l}^{-1}$  drop.